Optimization of a low-energy, high brightness electron gun for inverse photoemission spectrometers

S. Raj and D. D. Sarma[a)]
Solid State and Structural Chemistry Unit, Indian Institute of Science, Bangalore-560012, India

(Received 18 March 2003; accepted 21 December 2003; published 16 March 2004)

Availability of a low-energy, high current electron gun delivering a well-focused spot on the sample is essential for the inverse photoelectron spectroscopy. We have optimized an electron gun to obtain the maximum beam current at all electron kinetic energies of relevance with a reasonably small focus spot. Here we present the design, the procedure for the optimization, as well as the resulting characteristics of the electron gun. © *2004 American Institute of Physics.*
[DOI: 10.1063/1.1647694]

I. INTRODUCTION

Many experiments require electron beam with kinetic energies up to 100 eV. In particular, inverse photoemission spectroscopy (IPS) employing such low-energy electrons, in contrast to the same technique but using a high-energy electron source, has several advantages. For example, it is well known that the cross sections of all states usually decay rapidly with increasing kinetic energy of the incident electrons. The high-energy inverse photoemission technique suffers particularly from a very low cross section of *s* and *p* states compared to *d* and *f* states. Additionally, there can be significant damage caused to the sample surface by a high-energy electron beam. The combined effect of these factors makes the low-energy technique more suitable for studies on catalysis, surface science, most of the inorganic compounds, molecules, and semiconductors. At the low incident electron energy, it is possible to study surfaces and adsorbates by going below the threshold for electron stimulated desorption or decomposition. Also it is possible to obtain monolayer sensitivity due to the shorter electron mean free path of about 5 Å. Moreover, the high-energy technique is not at all suitable for angle-resolved measurements, since it is difficult to keep the momentum defined within a fraction of the Brillouin zone at such high energies due to the scaling of the momentum uncertainty with the square root of the kinetic energy with a fixed angular divergence; also, enhanced thermal scattering and the finite momentum of the photons contribute further uncertainties. Thus, low-energy inverse photoemission spectroscopy has become a powerful tool to study a wide range of problems. Among the two possible modes of operation for IPS, either by fixing the detecting photon energy, also known as the isochromat mode, or by keeping the incident electron energy constant, the isochromat mode with bandpass photon energy detectors is more common owing to its low cost and versatility. However, in this mode, it is absolutely essential to have a well characterized, low-energy electron gun, capable of delivering high current with a small focus spot on the sample. The production of low energy is limited by space charge effects due to the relatively low electric fields existing at the cathode surface.

Several gun designs for IPS can be found in the literature[1–3] but at the same time none of these designs satisfies all features required for IPS. In the present article, we adopt the dimensions of the gun as described by Stoffel and Johnson[3] to satisfy the geometry of a low-energy electron gun. It should be noted that the original design criterion[3] was to optimize the gun characteristics, such as the focus spot and the extracted current, for working at a fixed electron energy, namely 19 eV. The gun could also perform over the variable energy range of 5–30 eV, but with nonoptimal properties; specially, the current at the low-energy end is quite small due to space-charge limited conditions. One of the reasons for these limitations is that in the design presented in Ref. 3, the potential ratio between the extractor and the cathode is kept arbitrarily fixed at $V_e/V_c = 6:1$ for all the kinetic energy. In our design, we have experimentally optimized every potential over the range of relevant kinetic energies by taking all possible combinations of potentials in all electrodes and measuring the beam characteristics at the sample position. Ion and electron optics tracing software such as SIMION can in principle be used to get the required potentials for any kinetic energy; however, such programs cannot handle the space-charge effect, making it impossible to find out the optimized potentials for low kinetic energies from such simulations alone. Moreover, the actual realization of an electron gun is bound to have finite deviations from the ideal design due to various mechanical limitations. Such deviations from the actual geometry are also expected to affect the gun characteristics, particularly at the low-energy end, and cannot be accounted for in the simulation programs, making it necessary to seek experimental methods to optimize and characterize the specific electron gun. Our method of optimization and characterization will be helpful for any new electron gun design.

II. DESIGN

The design of the gun is schematically shown in Fig. 1. While designing, one of the requirements for the gun was

[a)]Author to whom correspondence should be addressed. Also at Jawaharlal Nehru Center for Advanced Scientific Research, Bangalore, and Center for Condensed Matter Theory, IISc; electronic mail: sarma@sscu.iisc.ernet.in

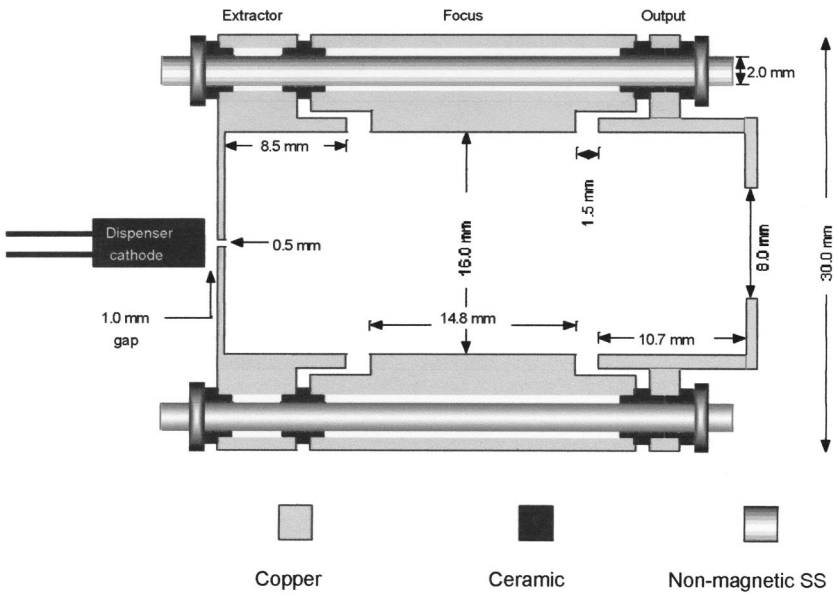

FIG. 1. The schematics diagram of the electron gun design.

that it should be as light as possible without compromising the mechanical strength as the gun has to be mounted with the help of three long stainless steel rods of 4 mm diameter from a flange with an electrical feedthrough. All the electrodes are machined from a pure copper rod as copper is one among few metals that do not poison the BaO-based cathode used as the electron source in the electron gun. The total length of the electron gun is about 38 mm. The distance between the front face of the electron gun and the sample is 20 mm. We have used a 3.4-mm-diam plane BaO dispenser cathode[4] as the electron emitter. The cathode operates at a low temperature, about 900 °C, emitting electrons with a narrow energy distribution (0.25 eV).[5] As described in the literature,[3] the electrons emerge from the anode aperture, appearing to originate from a point source placed behind the aperture at a distance equal to three times the actual cathode to anode distance; the angular spread of these electrons contains both the thermal and geometrical contributions.

The front surface of the BaO cathode is situated 1 mm behind the extractor. The BaO cathode is supported by tungsten wires, as tungsten does not cause poisoning of the BaO cathode.[6] All the electrodes are separated by ceramic spacers machined from machinable ceramics.[7] The design of the extractor, focusing, and output electrodes are made in such a way that no electron can see the ceramic parts used as spacers; otherwise, ceramic spacers tend to be charged up by low-energy electrons and distort the electric field profile inside the gun. All the electrodes are held together by three nonmagnetic stainless steel rods, resulting in a compact and mechanically stable structure. The gun is mounted on a CF 40 UHV flange with multi-pin electrical feedthrough and the CF 40 flange is mounted on a *Z*-shift assembly, which allows adjustment of the gun under the UHV condition.

III. CHARACTERIZATION

The electronic circuits needed for the operation of electron gun are described in Fig. 2. All the potentials for cathode, extractor, focusing and output electrodes, namely V_c, V_e, V_f, and V_o, can be independently tuned from -125 to $+125$ V through the programmable power supply. In the programmable power supply, we have used high-voltage operational amplifier (OPAMP) 3583 of Burr Brown in the inverting mode. This OPAMP has a wide range of voltage supply from ± 70 to ± 150 V and a maximum output current of 75 mA with $I_B = 20$ pA and thermal shutdown protection. This OPAMP is supplied with $+125$ V as V_{cc} and -125 V as $-V_{cc}$. The gain is adjusted by the ratio of resistors used in the circuit; in our application, we set R_2/R_1 to 12.5. The input voltages to all the four programmable power supplies are supplied from four independent computer-controlled 12 bit digital-to-analog converter outputs, each of which has a maximum range of ± 10 V. The use of independent programmable power supplies for each of the electron gun segments is in contrast to previously reported designs where fixed ratios between all the four potentials, namely V_c, V_e, V_f, and V_o, were assumed. As we shall show later, it is important to have independent voltage controls, particularly for the low-energy (5–15 eV) range, in order to overcome the limitations imposed by the space-charge effects.

We used a cross wire, made of a 2.5-mm-wide and 1-mm-thick copper strip, on an *XYZ* sample manipulator to measure the beam profile and the spot size. The total current at the sample stage was, however, collected on a larger plate grounded through a microammeter. In order to optimize the performance of the electron gun, we first measured the beam current taking all possible combinations of potentials in extractor, focusing, and output electrodes at a particular electron kinetic energy which is determined by V_c. We scanned the three voltages, V_e, V_f, and V_o over reasonably wide ranges with small steps using three nested loops in the control program of the power supply. To start with, we recorded typically 17 000 data points on a coarse grid of V_e, V_f, and V_o for any given kinetic energy. In Fig. 3 we show the measured beam current as a function of sequence of data points, each point denoting the unique sample current for a specific setting of V_e, V_f, and V_o for a 10 eV electron kinetic energy

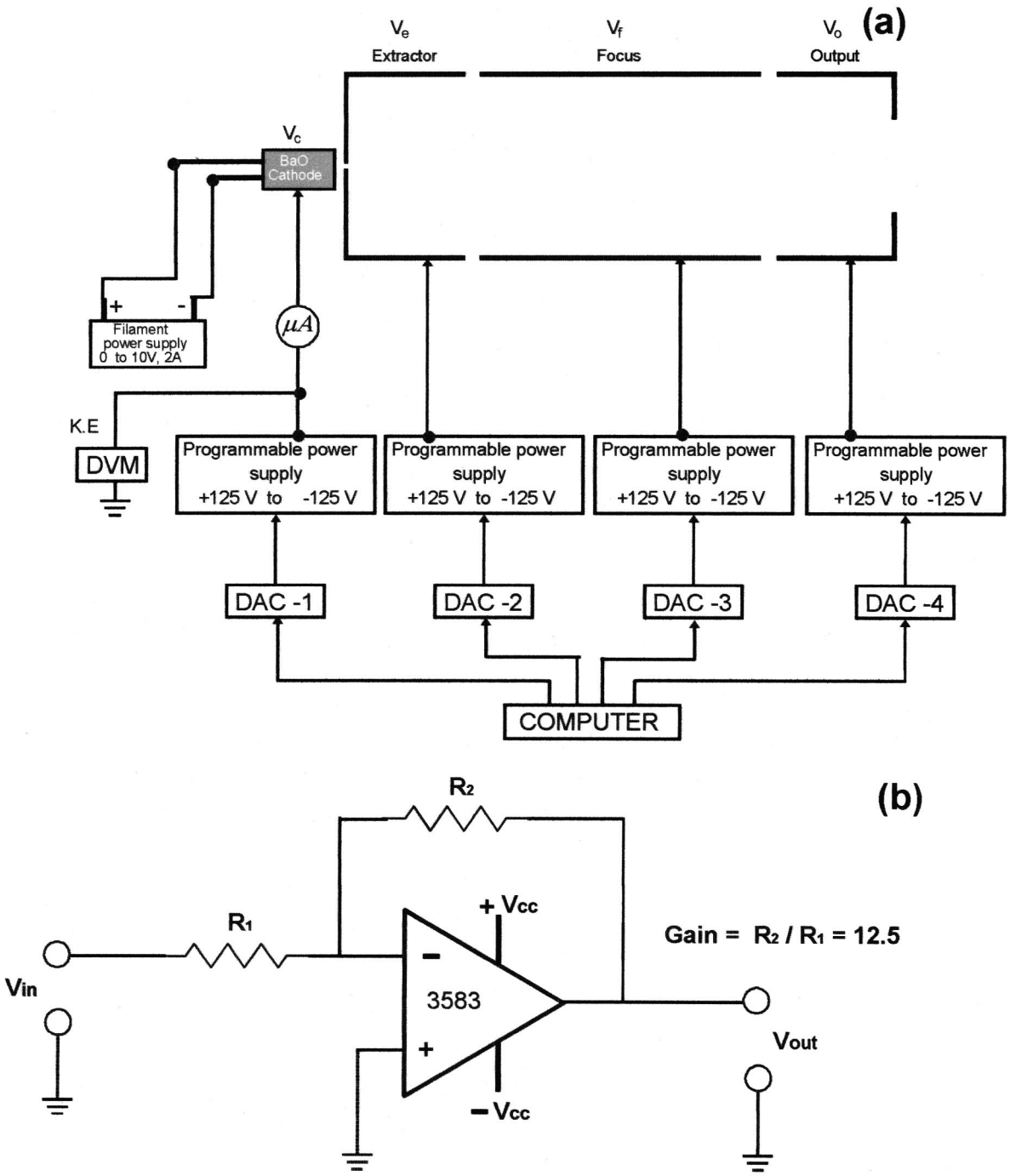

FIG. 2. (a) The electronic circuit diagram for power supply to all electrodes of the gun and (b) the required gain in our programmable power supply.

beam. The plot exhibits an approximately periodic behavior. Each of these peak structures in the beam current corresponds to a specific value of V_e; for example, the first structure is for $V_e = 50$ V and the last one for $V_e = 20$ V with the sample current varying as a function of V_f and V_o for a fixed V_e within each region. We find that the beam current maxima is a slowly decreasing function of V_e, exhibiting a total reduction of about 15% for a change of V_e from 50 to 20 V. Since our power supply is limited to a maximum of 125 V and we wish to have an approximately constant relationship between the kinetic energy and V_e, we choose $V_c : V_e$ to be 1:3 over the entire range of operation, 10 eV$\leqslant$KE$\leqslant$40 eV. This implies operating the gun at $V_e = 30$ V for KE$=$10 eV in Fig. 3, at which point the sample current is only 7% lower than the maximum achievable with $V_e = 50$ V (see Fig. 3). This minor decrease in the sample current is acceptable in view of the ease of operation in this mode. Interestingly, however, we find that the sample current maxima do not show a monotonic behavior with V_e for kinetic energies below 10 eV. Therefore, we have chosen the specific V_e values that maximize the sample current for KE$<$10 eV. In order to maximize the sample current with respect to the other two potentials, V_f and V_o, we inspect on a coarse grid the dependence of the sample current on these two potentials for the chosen V_e, as shown in Fig. 4 for KE$=$10 eV. As seen here, the sample current shows a broad, but clear maximum.

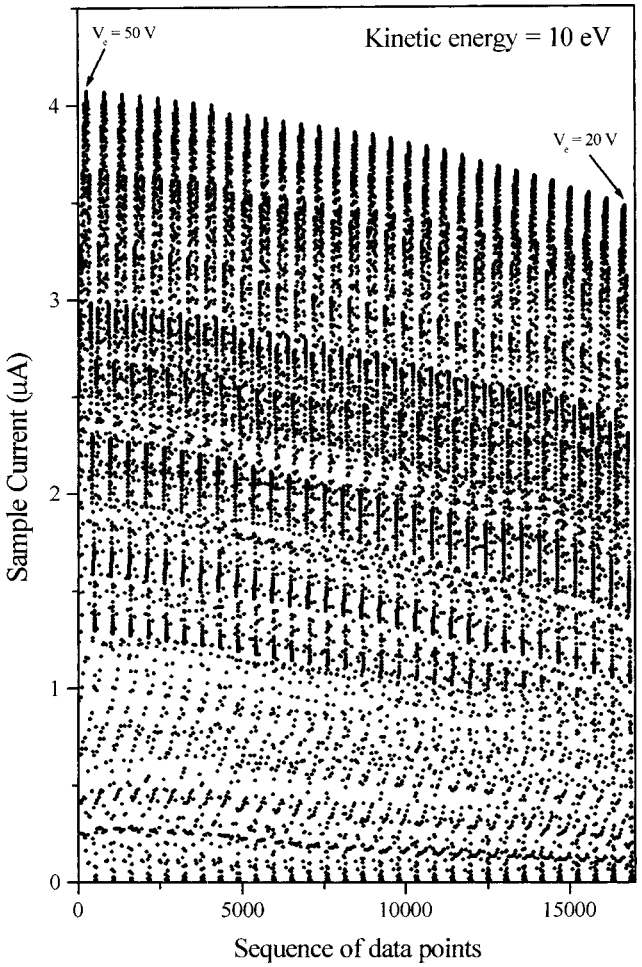

FIG. 3. The beam current as a function of sequence of data points, each point denoting the unique sample current for a specific setting of V_e, V_f, and V_o for a 10 eV electron kinetic energy beam.

We then carry out a fine grid search to maximize the beam current as a function of V_f and V_o. Table I gives the optimized potentials and in Fig. 5 we plot these optimal choices of V_e, V_f, and V_o as a function of kinetic energy. We have also shown the approximate analytical forms of these optimized potentials as a function of kinetic energy and the corresponding continuous theoretical curves by solid lines. These analytical forms then allow us to decide on the optimal set of gun potentials for any arbitrary kinetic energy. Since the gun power supply has four independently controlled programmable power supplies, it is straightforward to set the potentials as obtained here.

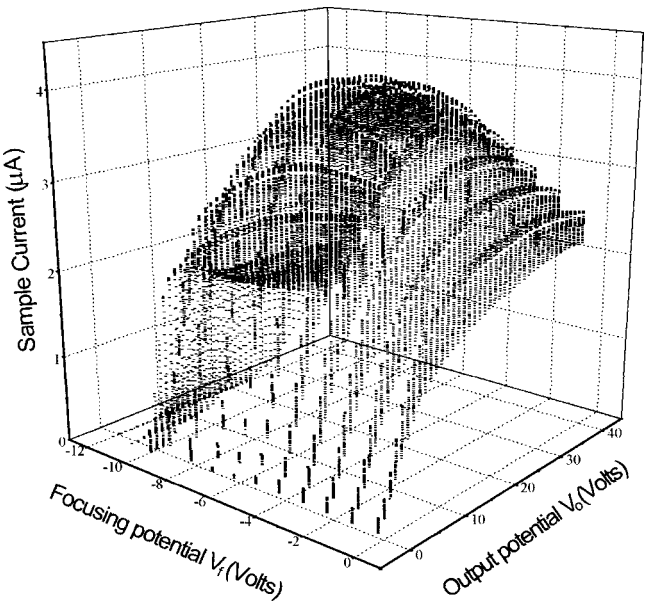

FIG. 4. The optimal potentials for V_f and V_o for 10 eV kinetic energy beam.

TABLE I. Optimized potentials for different kinetic energies.

KE (eV)	V_c (Volts)	V_e (Volts)	V_f (Volts)	V_o (Volts)
5	−5	25	−2.8	21.8
8	−8	28	−4.5	22.0
10	−10	30	−6.5	21.0
15	−15	45	−12.1	7.8
20	−20	60	−16.9	0
25	−25	75	−21	0
30	−30	90	−25.2	0
35	−35	105	−29.4	0
40	−40	120	−33.6	0

In order to fully characterize the electron gun operating with these optimized electrode potentials, we have measured the total beam current as a function of kinetic energy at different filament currents (Fig. 6). In the low-energy range (5–15 eV), the current increases rapidly and then becomes almost constant for higher kinetic energies; the constant current levels at higher kinetic energies are 2.5, 4.5, and 8.0 μA

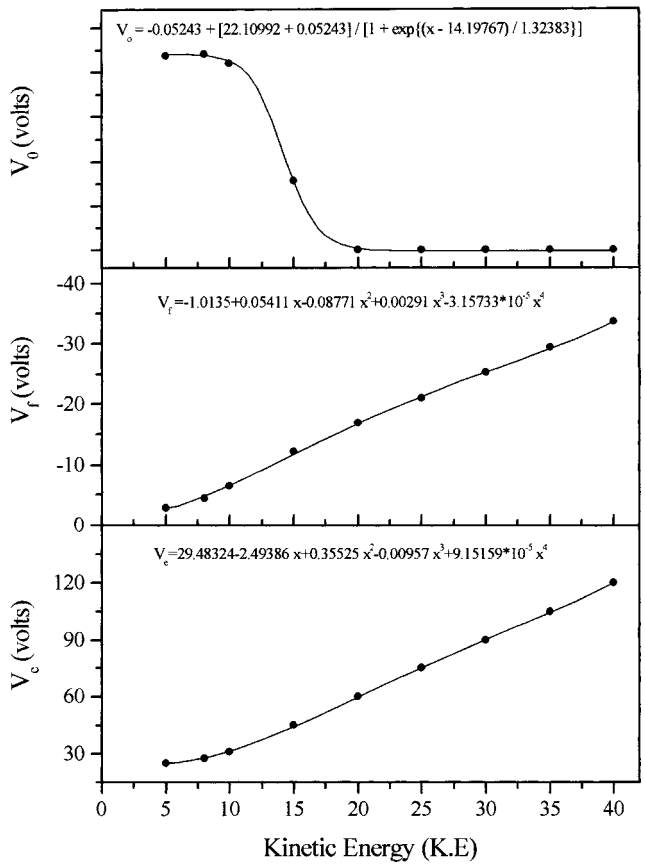

FIG. 5. The optimal choices of V_e, V_f, and V_o as a function of the kinetic energy.

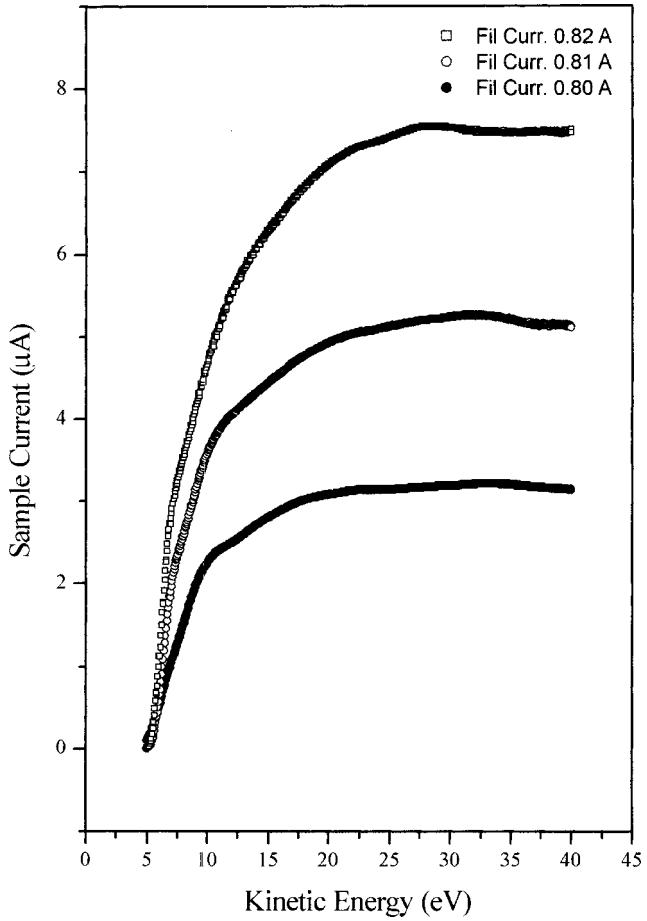

FIG. 6. Total beam current as a function of kinetic energy at different filament currents.

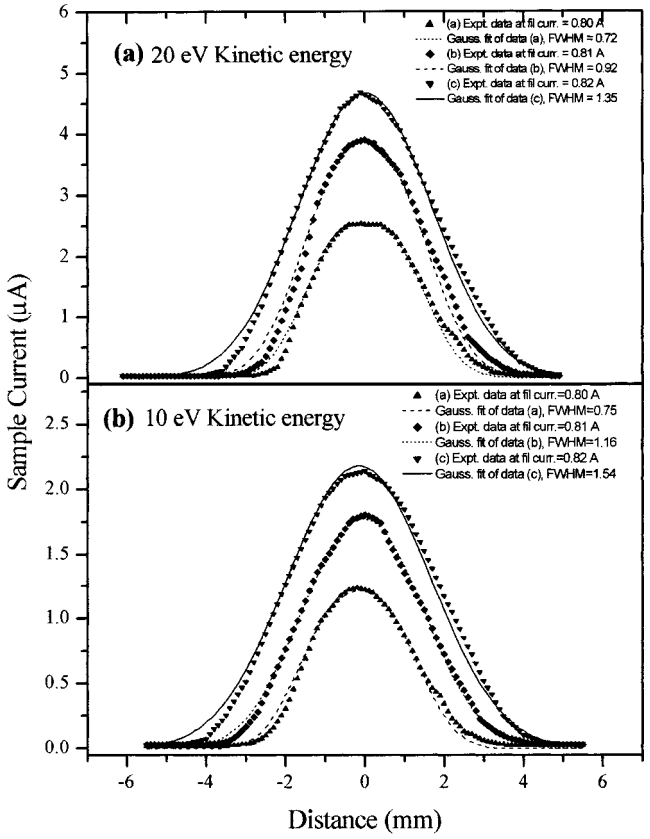

FIG. 7. (a) and (b) Beam profile of 20 and 10 eV kinetic energy at different filament currents.

for filament currents of 0.80, 0.81, and 0.82 A, respectively. In order to characterize the electron beam, not only in terms of total beam current shown in Fig. 6, but also in terms of the spot size on the sample, we have used the thin strip of copper to collect the current. The current collected this way is measured while moving the copper strip along a line perpendicular to the gun axis, such that the electron beam traverses across the width of the collector as a function of the position of the copper piece. We plot the measured current as a function of the position of the collector for three different filament currents and two different kinetic energies in Figs. 7(a) and 7(b). The electron current profiles clearly show an increase of the spot size with increasing beam current arising from an enhanced filament current at any given kinetic energy by the enhanced spread of the profiles. This is easy to understand in terms of space-charge effects, since this factor becomes more manifest with increasing total current. Additionally, we notice that the spot size is larger at the lower kinetic energy of 10 eV compared to that at the higher kinetic energy of 20 eV [see Figs. 7(a) and 7(b)] for a fixed filament current; this is also understandable in terms of the space-charge effect. We find that the spot size does not depend appreciably on the kinetic energy for larger kinetic energies.

It should be noted that the actual spot size cannot be directly estimated from the spread or the full width at half maxima (FWHM) of the current profiles in Fig. 7, as the total spread is contributed by the finite width of the collector strip. Assuming the intrinsic electron spot to have a Gaussian profile, the measured profile is approximately given by the convolution of a rectangular function representing the effective width of the collector and the Gaussian function representing the spot profile. Thus, we have fitted all the measured profiles in Fig. 7 by the convolution of the rectangular function of known width and a Gaussian function whose FWHM was varied to obtain the best fit to the experimental data within a least-squared-error approach. The resulting best fits shown by the solid and dashed lines are overlayed on the experimental data points. We have also shown the corresponding FWHMs of the Gaussians that provide quantitative estimates of the spot sizes obtained with this gun under the optimal condition of usage.

It should be noted that the performance of the gun has been optimized to deliver the maximum current, while integrating the total current over a large area. Of course, the results in Fig. 7 show that spot sizes under the optimized voltage conditions are reasonably small; however, it does not establish the optimized voltage conditions to be necessarily also optimal from the spot-size considerations. In order to obtain the optimized voltage conditions for the smallest spot size, we carried out a large number of independent studies to determine the spot size as a function of the various voltages. We show in Figs. 8 and 9 the spot size variation as a function of V_f and V_o keeping the extractor voltage V_e constant for 20 and 10 eV kinetic energies, respectively. Figures 8(a) and 9(a) show the profile of the beam at a few selected settings.

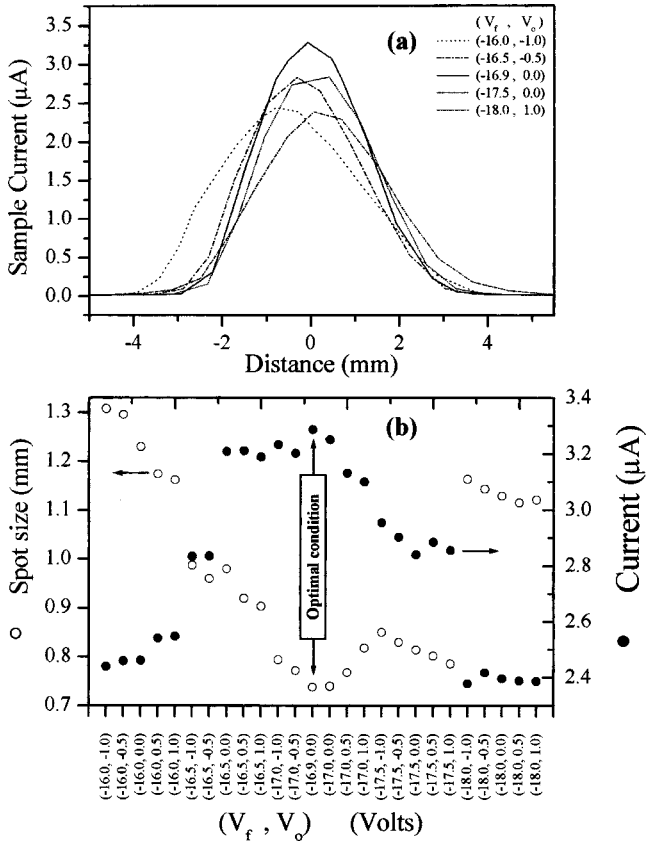

FIG. 8. (a) Stability of beam at 20 eV kinetic energy and (b) the beam current and spot size for different combination of (V_f, V_o).

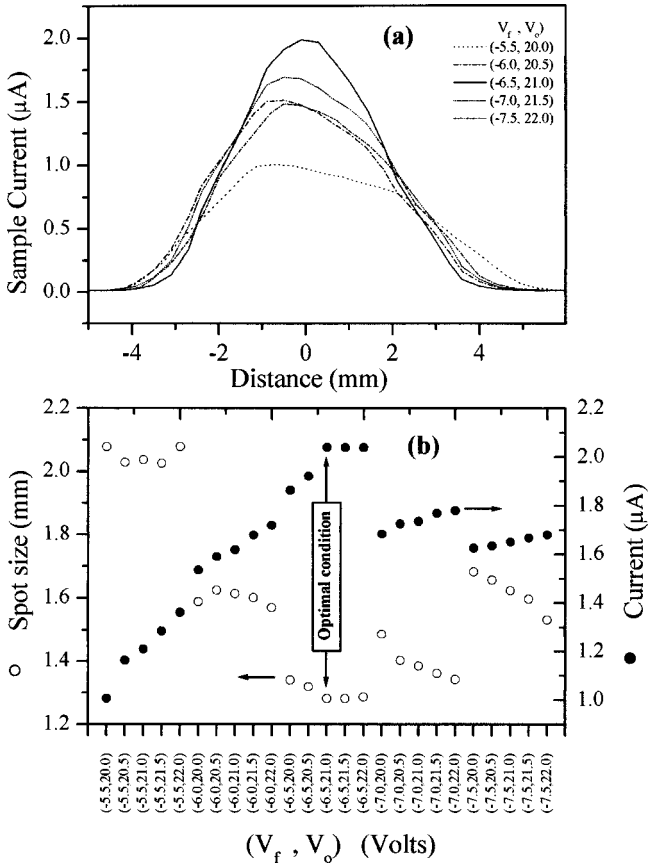

FIG. 9. (a) Stability of beam at 10 eV kinetic energy and (b) the beam current and spot size for different combinations of (V_f, V_o).

From these figures, it is clear that the centroid of electron beam moves by ± 0.4 mm [Fig. 8(a)] and ± 0.2 mm [Fig. 9(a)] from its mean position due to different potentials at the focus and output electrodes, thereby illustrating the overall stability of the beam position under different operating conditions. Figures 8(b) and 9(b) show the spot size for different combinations of (V_f, V_o); in the same plot we also show the total beam current obtained at these settings. It is clear from the figures that for the highest optimized value of the beam current, the beam size is also the smallest in both the figures. This establishes that the present procedure simultaneously optimizes both the beam current and the spot size over the relevant range of kinetic energy.

These considerations suggest that this design provides a well focused and reasonably high intensity electron beam over the entire range of kinetic energies for which it is designed. In terms of perveance, $P_{\max}=I_{\max}/V^{3/2}$ indicates the maximum current $I_{\max}$ which can be provided before space-charge effect either prevents further current increase or causes undesirable effects in the beam. An increase in perveance causes the beam size to increase due to space-charge effect. From Fig. 7, we find that the beam width changes from 0.72 to 1.35 mm for a change in the perveance from 0.035 to 0.08 μperv for 20 eV electron kinetic energy. Similarly for 10 eV electron kinetic energy the beam width changes from 0.75 to 1.54 mm for the change of perveance from 0.07 to 0.14 μperv. As our gun is lightweight and gives required current also at the low kinetic energy end, it satisfies all the requirements for experiments using inverse photoelectron technique.

ACKNOWLEDGMENTS

This work is funded by the Department of Science and Technology and the Council of Scientific and Industrial Research, Government of India.

[1] J. A. Simpson and C. E. Kuyatt, Rev. Sci. Instrum. **34**, 265 (1963).
[2] P. W. Erdman and E. C. Zipf, Rev. Sci. Instrum. **53**, 225 (1982).
[3] N. G. Stoffel and P. D. Johnson, Nucl. Instrum. Methods Phys. Res. A **234**, 230 (1995).
[4] Procured from Spectra-Mat, Inc., 1240 Highway 1, Watsonville, California 95076.
[5] W. Franzen and J. H. Porter, Adv. Electron. Electron Phys. **39**, 73 (1975).
[6] J. L. Cronin, IEE Proc., Part I: Solid-State Electron Devices **128**, 19 (1981).
[7] Machineable ceramics, Procured from MDC, UK.